

Bismuth Trioxide Modified Carbon Nanotubes as Negative Electrode Catalysts for all Vanadium Redox Flow Batteries

Youqun Chu*, Haixia Zhou, Huimin Zhao

State Key Laboratory Breeding Base of Green Chemistry-Synthesis Technology,
Chemical Engineering College, Zhejiang University of Technology, Hangzhou 310014, China

*E-mail: chuyq@zjut.edu.cn

Received: 12 March 2020 / Accepted: 24 May 2020 / Published: 10 July 2020

Bismuth trioxide modified carbon nanotubes ($\text{Bi}_2\text{O}_3/\text{CNTs}$) composite was fabricated by liquid phase deposition-calcinating method and used as electrocatalyst for $\text{V}^{3+}/\text{V}^{2+}$ redox couple of all vanadium redox flow batteries (VRFBs). The modification of Bi species at the surface of CNTs can significantly inhibit the hydrogen evolution reaction and enhance the electrochemical activity to the $\text{V}^{2+}/\text{V}^{3+}$ redox reaction. The VRFB single cell with $\text{Bi}_2\text{O}_3/\text{CNTs}$ modified graphite felt as negative electrode exhibits excellent energy storage performances, such as higher charge/discharge capacity and energy efficiency, indicating that the $\text{V}^{2+}/\text{V}^{3+}$ redox reaction can be facilitated significantly by $\text{Bi}_2\text{O}_3/\text{MWCNTs}$ composite.

Keywords: bismuth trioxide; carbon nanotubes; vanadium redox flow batteries; hydrogen evolution overpotential

1. INTRODUCTION

All vanadium redox flow batteries (VRFBs), combined with the advantages of long cycle life, independent power and capacity, reduced crossover effect by employing the same vanadium element electrolytes, *etc.*, have been proved to be one of the most promising energy storage systems [1-4]. Despite the above compelling merits, VRFBs have achieved only limited market presence up to now [5]. The battery performances, such as energy density, power density and capacity retention, need to be further improved to meet the requirements of the practical application.

During the past decades, tremendous efforts including the development of electrolytes[6,7], membranes[8,9] and electrodes[10-14], have been made to improve the battery performance. As yet, graphite felt (GF) is the most widely used electrode material for VRFBs. In order to enhance the electrochemical activity of GF, lots of treating methods have been developed, such as heat treatment[8], acid treatment[15-17], electrochemical oxidation[18,19] and modification by noble metal

catalysts[8,20,21], *etc.* Most of the literatures concerning electrode materials for VRFBs are focused on investigating and improving the positive half-cell electrode, while only few deal with the negative electrode[22-25]. Due to the low hydrogen evolution overpotential of carbon-based materials in acidic solutions[26], the loss of charge/discharge efficiencies and the charge imbalance between positive and negative electrolytes caused by the parasitic side reaction of hydrogen evolution at negative electrode are worsening with the prolonging of charge/discharge cycles[27]. At present, avoiding the states of charge greater than 0.85 or the use of electrolyte rebalancing devices are the commonly adopted strategies to alleviate the effect of hydrogen evolution reaction[28,29]. Little attention has been paid to inhibit the hydrogen evolution reaction by modification the negative electrode.

Recently, the graphite felt modified with bismuth has been reported as a robust negative electrode for VRFBs[30,31]. The introducing of bismuth can significantly improve reversibility of V^{2+}/V^{3+} redox reaction and inhibit the hydrogen evolution reaction simultaneously. This finding can be considered as a breakthrough for the development of high-performance negative electrode of VRFBs. Nevertheless, further studies are necessary to verify the electrocatalytic activity of bismuth component with different support, which benefits to enhance the performance of VRFBs.

Multi-walled carbon nanotubes (CNTs) have been proved as good electrocatalysts and supports for both positive and negative electrodes of VRFBs, introducing bismuth species onto the surface of CNTs is expected to be an effective way to obtain a powerful electrocatalyst for the negative electrode of VRFB. Hence bismuth trioxide modified CNTs ($Bi_2O_3/CNTs$) were prepared by liquid phase deposition method in the present paper. The surface morphology, microstructure and surface chemistry of $Bi_2O_3/CNTs$ composites were investigated by a transmission electron microscopy (TEM) and X-ray diffraction (XRD). The alteration of electrocatalytic activity for CNTs and $Bi_2O_3/CNTs$ were investigated by cyclic voltammetry (CV), electrochemical impedance spectroscopy (EIS). VRFB performances of GF before and after modification with $Bi_2O_3/CNTs$ were investigated by VRFB single cell charge-discharge test. Finally, the dominant factors that affect the VRFB performance are identified by EIS of the VRFB single cell.

2. EXPERIMENTAL

2.1 Catalyst preparation

The catalyst was synthesized by liquid phase deposition-calcinating method. Briefly, 0.4 g CNTs were suspended in ethanol, then 5 mL $0.1 \text{ mol}\cdot\text{L}^{-1}$ $BiCl_3$ solution was added and mixed sufficiently for 30 min. by ultrasonication. Subsequently, ammonia solution was added drop by drop and stirred for 6 h. After the synthesis, the precursor powders were collected by vacuum filtration and washed three times with deionized water and three times with ethanol. The precursor powders were dried in vacuum oven at $70 \text{ }^\circ\text{C}$, then calcined under N_2 atmosphere in a tube furnace at $500 \text{ }^\circ\text{C}$ for 4 h prior to use it for catalytic reaction. The obtained catalyst-modified GFs were used as negative electrodes in VRFBs.

2.2 Characterization

The crystalline structure was investigated by an X-ray Diffractometer (Thermo ARL SCINTAG X-TRA) using Cu K_{α} radiation. The morphology of catalyst was determined by a Tecnai G2 F30 S-Twin TEM (Philips-FEI, The Netherlands).

2.3 Electrochemical testing

The linear scan voltammetry (LSV), cyclic voltammetry (CV) and electrochemical impedance spectroscopy (EIS) were conducted in a three-electrode cell using an IviumStat workstation (Ivium Technologies, The Netherlands). A graphite plate and a saturated calomel electrode (SCE) were used as the counter and reference electrodes, respectively. The working electrodes were prepared by applying highly dispersed $\text{Bi}_2\text{O}_3/\text{CNTs}$ ink onto the polished glassy carbon electrode (ϕ 3 mm). The ink was prepared by dispersing 10 mg $\text{Bi}_2\text{O}_3/\text{CNTs}$ in the 20 μL 5 wt% Nafion emulsion and 0.5 mL isopropanol under strong ultrasonication. The active materials loading on the disk electrode is 0.19 mg. The solution consisted of 1.5 $\text{mol}\cdot\text{L}^{-1}$ V^{3+} in 3.0 $\text{mol}\cdot\text{L}^{-1}$ H_2SO_4 . EIS measurements were performed at -0.3 V (vs. SCE) by applying an alternating voltage of 5 mV over the frequency ranging from 0.1 Hz to 100 kHz. Before each measurement, the electrode was immersed into the electrolyte for 2 h and the solution was purged with N_2 for 15 min. to eliminate the influence of dissolved oxygen.

2.4 VRFB single cell performance

GFs with an area of 3×3 cm^2 and thickness of 5 mm (Shenhe Carbon Fiber Materials Co., China) were treated in air at 500 $^{\circ}\text{C}$ for 2 h to improve the electrocatalytic activity and hydrophilicity. 25 mg $\text{Bi}_2\text{O}_3/\text{CNTs}$ was dispersed in the 100 μL 5 wt% Nafion emulsion and 10 mL isopropanol under strong ultrasonication to form a uniform black ink. A piece of heat-treated GF was immersed in the black ink for 30 min., then dried in a vacuum oven at 70 $^{\circ}\text{C}$ for 2 h, which was denoted as a catalyst-modified GF. A VRFB single cell was fabricated by sandwiching a piece of Nepem115 perfluorinated ion-exchange membrane (Best Co., China) between two pieces of GFs, two piece of graphite plates were used as the current collectors. The heat-treated GF and catalyst-modified GF were used as the positive and negative electrodes, respectively. 20 mL 1.5 $\text{mol}\cdot\text{L}^{-1}$ V^{3+} + 3.0 $\text{mol}\cdot\text{L}^{-1}$ H_2SO_4 solution and 20 mL 1.5 $\text{mol}\cdot\text{L}^{-1}$ VO^{2+} + 3.0 $\text{mol}\cdot\text{L}^{-1}$ H_2SO_4 solution were used as negative and positive electrolytes, respectively. The electrolytes were cyclically pumped into the corresponding half-cell by two peristaltic pumps (BT100-1L, Baoding Longer Precision Pump Co., China) with a flow rate of 10 $\text{mL}\cdot\text{min}^{-1}$. The performances of VRFB were examined by charge-discharge cycles with 50 $\text{mA}\cdot\text{cm}^{-2}$ between 0.8 V and 1.65 V using a CT2001 battery test system (LANHE instrument, China) at room temperature.

3. RESULTS AND DISCUSSION

3.1 Characterization of CNTs and Bi₂O₃/CNTs

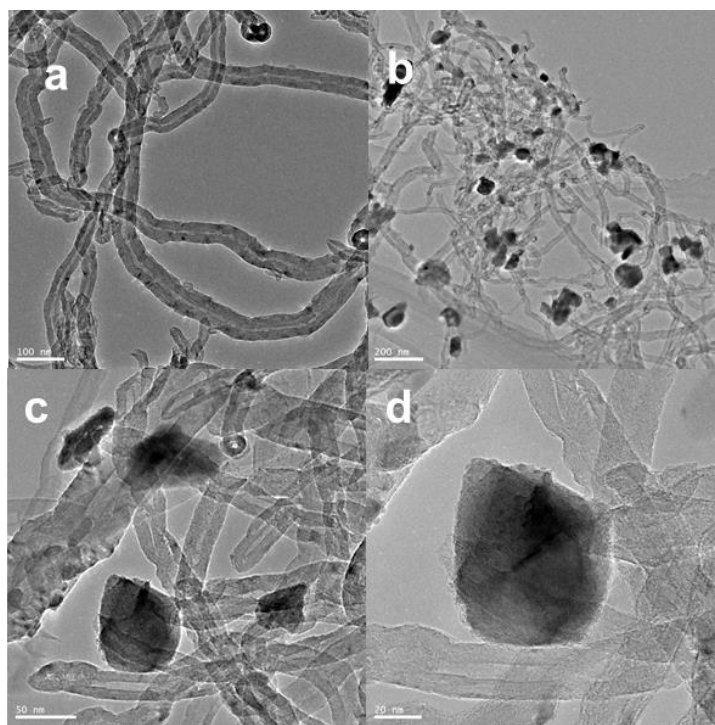


Figure 1. TEM images of CNTs (a) and Bi₂O₃/CNTs (b,c,d)

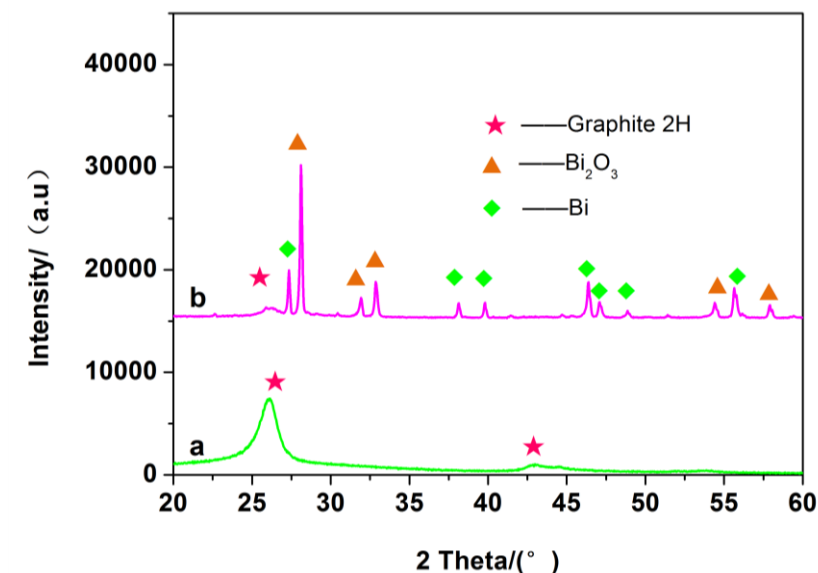


Figure 2. XRD patterns of CNTs (a), Bi₂O₃/CNTs (b)

The morphology and structure of the CNTs and Bi₂O₃/CNTs were analyzed by TEM. Fig. 1 shows images of CNTs and Bi₂O₃/CNTs. It can be seen from this figure that black nanosized particles are formed at the surface of CNTs after the modification of Bi species (Fig.1 b, c, d). The phase compositions of CNTs and Bi₂O₃/CNTs were investigated by XRD, as shown in Fig. 2. Only

characteristic diffraction peaks of CNTs can be seen from curve a, which implies the CNTs used in this work have high purity. After the modification of Bi species, diffraction peaks at 27.9° , 31.71° , 32.76° , 37.8° , 55.22° , 57.77° corresponding to the characteristic planes of (201), (002), (220), (222) and (402) of monoclinic Bi_2O_3 (JCPDS No. 76-1730) and relative weak peaks at 27.24° , 38.09° , 39.72° , 48.83° , 56.21° corresponding to the planes of (012), (104), (110), (202), (024) of Bi with hexagonal system (JCPDS No. 44-1246) can be observed. The existing of Bi in the composites can be ascribed to the reduction of Bi_2O_3 by carbon during the calcinating process[32].

3.2 Quasi-steady state polarization

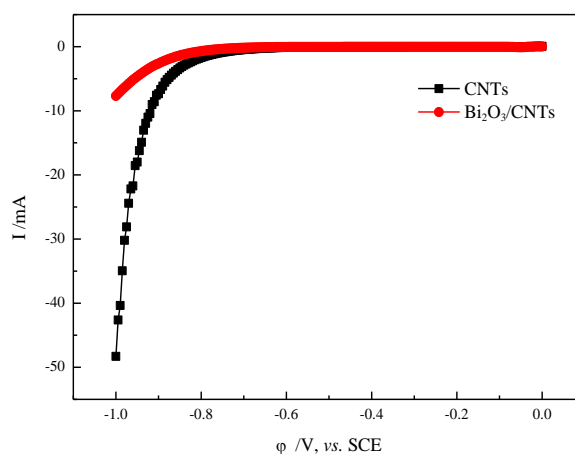


Figure 3. Quasi steady state polarization curves of CNTs and $\text{Bi}_2\text{O}_3/\text{CNTs}$ electrodes Electrolyte: $3 \text{ mol}\cdot\text{L}^{-1} \text{ H}_2\text{SO}_4$; scan rate: $1 \text{ mV}\cdot\text{s}^{-1}$

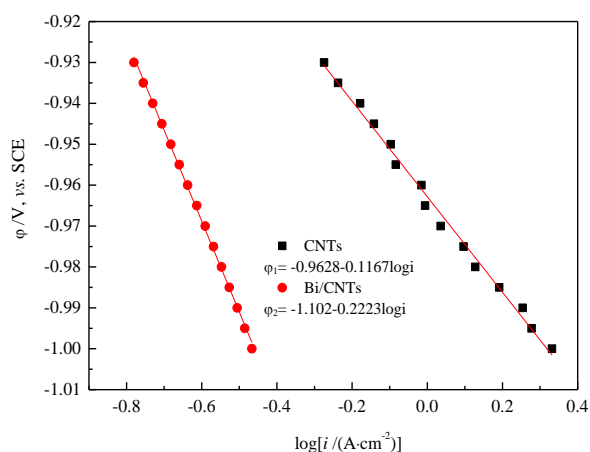


Figure 4. Tafel plots of CNTs and $\text{Bi}_2\text{O}_3/\text{CNTs}$ electrodes

In order to evaluate the inhibition abilities of Bi species to hydrogen evolution reaction, slow linear scan voltammetry (SLSV) as a quasi-steady state polarization method was conducted in $3 \text{ mol}\cdot\text{L}^{-1} \text{ H}_2\text{SO}_4$ at $1 \text{ mV}\cdot\text{s}^{-1}$. It can be seen from Fig. 3 that the hydrogen evolution reaction was significantly inhibited on $\text{Bi}_2\text{O}_3/\text{CNTs}$ compared to that of CNTs. The Tafel plots, shown in Fig. 4, were obtained

using the SLSV data from -0.93 V to -1.0V. Good linear relations are obtained between potential and logarithm of current density for CNTs and Bi₂O₃/CNTs electrodes. The potentials of hydrogen evolution reaction on CNTs and Bi₂O₃/CNTs electrodes at 1 A·cm⁻² are -0.9628 V and -1.102 V, respectively. This suggests that the hydrogen evolution reaction is inhibited after the introduced of Bi species on the surface of CNTs, and high charge/discharge efficiency can be expected when Bi₂O₃/CNTs used as the electrocatalyst for the negative electrode of VRFBs.

3.3 Cyclic voltammetry

Fig.5 shows the cyclic voltammograms of CNTs and Bi₂O₃/CNTs electrodes obtained in 1.5 mol·L⁻¹ V³⁺+3 mol·L⁻¹ H₂SO₄ at different potential scan rate. A pair of redox current peaks can be observed from the cyclic voltammograms of both electrodes, which corresponds to the redox reaction of V³⁺/V²⁺ couple. The peak potential shifts in the direction of potential scanning with the increasing of scan rate, which implies the characteristics of quasi reversible reaction of V³⁺/V²⁺ couple on both electrodes. In addition, the currents of oxidation peaks and reduction peaks for both electrodes present a good linear relationship with the square root of scan rate. This suggests the electrode processes on both electrodes are controlled by the mass transfer. The formal potential ($\varphi_f = \frac{\varphi_{pa} + \varphi_{pc}}{2}$) estimated from the anodic peak potential (φ_{pa}) and cathodic peak potential (φ_{pc}) of CV curves for Bi₂O₃/CNTs electrode is *ca.* -0.283 V which is higher than that of CNTs electrode (*ca.* -0.316 V). This implies the redox reaction of V³⁺/V²⁺ couple can take place more easily on Bi₂O₃/CNTs electrode. And the higher formal potential of V³⁺/V²⁺ couple on Bi₂O₃/CNTs electrode is more favorable to inhibit the occurrence of hydrogen evolution reaction. Moreover, the redox peak currents at Bi₂O₃/CNTs electrode are approximately 3 times of those at CNTs electrode. This indicates that the Bi species have good electrocatalytic activity to the redox of V³⁺/V²⁺ couple. Similar results have been reported on the electrocatalytic activity of Bi species supported on graphite felts to the redox of V³⁺/V²⁺ couple in the literatures[23,30,31,33,34]. Because CNTs have higher electrical conductivity than graphite felts, Bi₂O₃/CNTs shows excellent electrochemical performance as the electrocatalyst of V³⁺/V²⁺ couple.

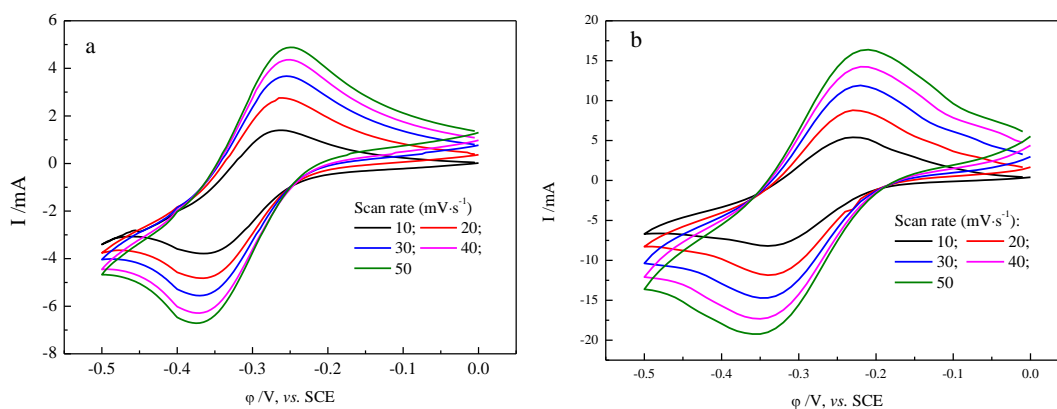


Figure 5. Cyclic voltammograms of CNTs (a) and Bi₂O₃/CNTs (b) under different scan rate in 1.5 mol·L⁻¹ V³⁺+3 mol·L⁻¹ H₂SO₄ electrolyte.

3.4 Electrochemical impedance spectroscopy

To further verify the electrocatalytic activity of Bi species on the redox reaction of V^{2+}/V^{3+} couple, EIS measurements under -0.2 V were conducted. Fig.6 shows Nyquist curves obtained on CNTs and $Bi_2O_3/CNTs$ electrodes in $1.5 \text{ mol}\cdot\text{L}^{-1} V^{3+} + 3 \text{ mol}\cdot\text{L}^{-1} H_2SO_4$ solution at -0.2 V. It can be seen from the figure that both Nyquist curves consist of two parts; The arcs at the high frequencies are corresponding to the charge transfer process, while the parts at low frequencies can be attributed to the Nernst finite diffusion process within the porous electrode. It can be inferred that the electrochemical process at both electrodes is simultaneously controlled by charge transfer and diffusion process[33, 35]. The Nyquist curves are fitted using the equivalent circuit shown in the inset of Fig. 6, where R_1 , R_2 and R_3 correspond to the ohmic resistance of the electrode materials and the electrolyte between the electrode surface and the luggin capillary, charge transfer resistance of V^{3+}/V^{2+} couple and finite diffusion resistance of vanadium ions between the electrode surface and the bulk solution, respectively. The electric double layer capacitance and the diffusion capacitance caused by the diffusion of vanadium ions in pore channel of the electrodes are represented by the constant phase elements CPE_1 and CPE_2 , respectively. The impedance of the constant phase element can be calculated by $Z_{CPE} = \frac{1}{Y_0} (j\omega)^{-n}$. The fitting results are listed in Table 1. It can be seen that $Bi_2O_3/CNTs$ electrode has much smaller R_1 , comparing with that of CNTs electrode. This can be ascribed to the good conductivity and hydrophilicity of $Bi_2O_3/CNTs$. The CNTs electrode has a relatively larger R_2 , 4.411Ω , which decreases to 2.417Ω after the introduction of Bi species onto the surface of CNTs. This implies that Bi species can enhance the redox reaction kinetics of V^{3+}/V^{2+} couple by accelerating the charge transfer process. These results are in good agreement with those obtained by the cyclic voltammetric experiments.

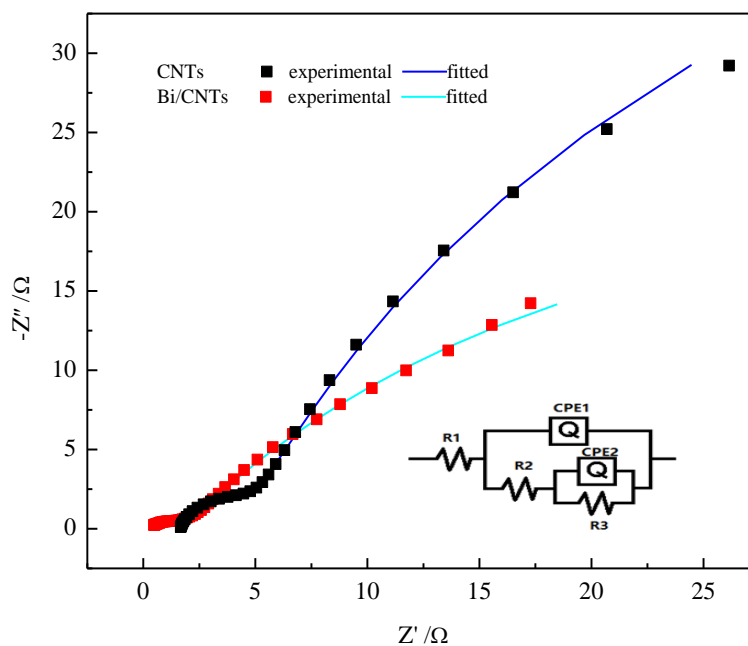


Figure 6. Nyquist curves recorded on CNTs and $Bi_2O_3/CNTs$ electrodes in $1.5 \text{ mol}\cdot\text{L}^{-1} V^{3+} + 3 \text{ mol}\cdot\text{L}^{-1} H_2SO_4$ solution at -0.2 V

Table 1. Kinetic parameters of electrochemical impedance spectroscopy

Catalyst	R_1/Ω	CPE ₁		R_2/Ω	CPE ₂		R_3/Ω
		$Y_0/\Omega^{-1}\cdot s^n$	n		$Y_0/\Omega^{-1}\cdot s^n$	n	
CNTs	1.65	0.0004165	0.8823	4.411	0.003516	0.8363	93.84
Bi/CNTs	0.1384	0.01162	0.4582	2.417	0.03661	0.6485	73.6

3.5 Charge/discharge performance

The effect of Bi species on the performance of VRFB single cells was investigated by galvanostatic charge/discharge method at $50 \text{ mA}\cdot\text{cm}^{-2}$. Fig.7a shows the typical charge/discharge profiles of the VRFB single cells assembled with CNTs and $\text{Bi}_2\text{O}_3/\text{CNTs}$ modified GFs as negative electrodes. The overpotentials for the cell with $\text{Bi}_2\text{O}_3/\text{CNTs}$ modified GF negative electrode decrease remarkably in the corresponding charge/discharge processes, compared with those of the cell with CNTs modified negative electrode. This can be ascribed to the enhanced electrocatalytic activity with the introduction of Bi species, resulting in lower charge voltage and higher discharge voltage and higher charge/discharge capacities (Fig.7b). In addition, it can be seen from Fig. 7b that the charge/discharge capacities of both batteries increase at the initial cycles, then decrease gradually after reaching the summit, which is especially obviously for the VRFB with $\text{Bi}_2\text{O}_3/\text{CNTs}$. This may be related to the non-equilibrium penetration of vanadium cations and water through the ion-exchange membrane and hydrogen evolution side reaction occurred at the end stage of charge process[36]. Due to the higher permeability of the vanadium ions with lower valence[37-39], the VO_2^+ ions formed in the positive electrolyte during the charge process react with the transferred V^{3+} and V^{2+} ions, resulting in the accumulation of vanadium ions with low valence. Thus, the discharge capacity depends on the concentration of available VO_2^+ ions in the positive electrolyte, and part of V^{2+} ions in the negative electrolyte cannot participate in the discharge reaction owing to the lack of VO_2^+ ions. With the decrease of vanadium ions in the negative electrolyte, the net transfer of low vanadium ions to the positive electrolyte decreases in the subsequent charge/discharge cycle. This may be the reason for the gradual increase of charge/discharge capacities of the VRFBs. When the vanadium ions in the negative electrolyte decrease to a certain value, the capacity of the VRFB is converted to a negative limitation, and decreases with the further decrease of vanadium ions. The cell with $\text{Bi}_2\text{O}_3/\text{CNTs}$ has higher charge/discharge capacities than that with CNTs, which can be ascribed to the electrocatalysis of Bi species. Due to the limitation of charge/discharge cut-off voltage, similar current efficiency ($\sim 95\%$, Fig.7c) can be obtained by both VRFBs. However, the cell with $\text{Bi}_2\text{O}_3/\text{CNTs}$ exhibits a little higher energy efficiency than that with CNTs (Fig.7d). This further confirmed the good electrocatalytic activity of $\text{Bi}_2\text{O}_3/\text{CNTs}$ to the redox of $\text{V}^{3+}/\text{V}^{2+}$ couple.

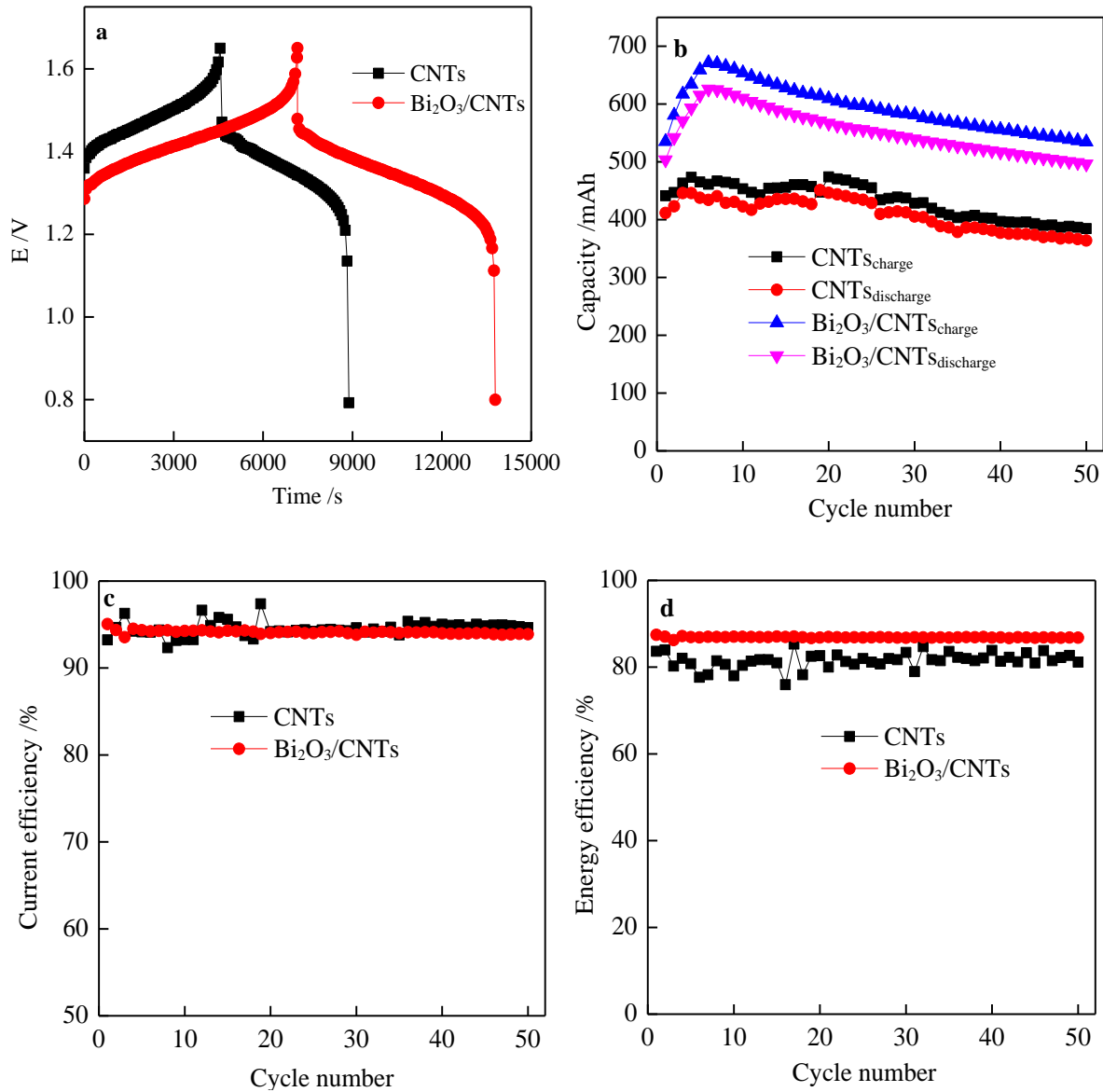


Figure 7. Electrochemical performance of VRFB single cells assembled with CNTs and Bi₂O₃/CNTs modified GFs as negative electrodes at 50 mA·cm⁻². (a) typical charge/discharge profiles; (b) capacity; (c) current efficiency; (d) energy efficiency

4. CONCLUSIONS

In this work, Bi₂O₃/CNTs composites were prepared by liquid phase deposition-calcinating method and their electrochemical performance were investigated. The experimental results show that the modification of Bi species at the surface of CNTs can significantly inhibit the hydrogen evolution reaction, and enhance the electrochemical activities to the V²⁺/V³⁺ redox couple. The VRFB single cell with Bi₂O₃/CNTs modified GF as negative electrode exhibits excellent energy storage performances, such as higher charge/discharge capacity and energy efficiency, indicating that the V²⁺/V³⁺ redox reactions can be facilitated significantly by Bi₂O₃/CNTs composite.

ACKNOWLEDGEMENTS

This work is partially supported by the National Key Research and Development Program of China (2017YFB0307503) and Innovation Team Project of Science Technology Department of Zhejiang Province (2011R09002-05).

References

1. E. Sum, M. Rychcik, M. Skyllas-Kazacos, *J. Power Sources*, 16(1985)85.
2. E. Sum, M. Skyllas-Kazacos, *J. Power Sources*, 15 (1985) 179.
3. M. Skyllas-Kazacos, M. Rychcik, R.G. Robins, A. G. Fane, M. A. Green, *J. Electrochem. Soc.*, 133(1986)1057.
4. B. Dunn, H. Kamath, J. M. Tarascon, *Science*, 334 (2011) 928.
5. K. Lourenssen, J. Williams, F. Ahmadpour, R. Clemmer, S. Tasnim, *J. Energy Storage*, 25(2019)100844.
6. P. K. Leung, M. R. Mohamed, A. A. Shah, Q. Xu, M. B. Conde-Duran, *J. Power Sources*, 274(2015)651.
7. X. W. Wu, J. Liu, X. J. Xiang, J. Zhang, J. P. Hu, Y. P. Wu, *Pure Appl. Chem.*, 86(2014)661.
8. B. T. Sun, M. Skyllas-Kazacos, *Electrochim. Acta*, 36(1991) 513.
9. J. Y. Ye, C. Wu, W. Qin, F. F. Zhong, M. Ding, *J. Nanosci. Nanotechnol.*, 20(2020)4714.
10. M. Park, J. Ryu, J. Cho, *Chem. Asian J.*, 10(2015)2096.
11. O. D. Blasi, N. Briguglio, C. Busacca, M. Ferraro, V. Antonucci, A. D. Blasi, *Appl. Energy*, 147(2015)74.
12. D. Chen, M. A. Hickner, E. Agar, E. C. Kumbur, *ACS Appl. Mater. Inter.*, 5(2013)7559.
13. S. N. Yang, Y. Cheng, X. Xiao, H. Peng, *Chem. Eng. J.*, 384(2020)123294.
14. M. R. Mohamed, P. K. Leung, M. H. Sulaiman, *Appl. Energy*, 137(2015)402.
15. B. T. Sun, M. Skyllas-Kazacos, *Electrochim. Acta*, 37(1992) 2459.
16. Y. Men, T. Sun, *Int. J. Electrochem. Sci.*, 7(2012)3482.
17. L. Yue, W. S. Li, F. Q. Sun, L. Z. Zhao, L. D. Xing, *Carbon*, 48 (2010)3079.
18. W. Zhang, J. Xi, Z. Li, H. Zhou, L. Liu, Z. Wu, X. Qiu, *Electrochim. Acta*, 89(2013)429.
19. X. G. Li, K. L. Huang, N. Tan, S. Q. Liu, L. Q. Chen, *J. Inorg. Mater.*, 21(2006) 1114.
20. W. H. Wang, X. D. Wang, *Electrochim. Acta*, 52(2007)6755.
21. C. Flox, J. Rubio-Garcia, R. Nafria, R. Zamani, M. Skoumal, T. Andreu, J. Arbiol, A. Cabot, J. R. Morante, *Carbon*, 50(2012)2372.
22. E. Agar, C. R. Dennison, K. W. Knehr, E. C. Kumbur, *J. Power Sources*, 225(2013)89.
23. J. S. David, G. Zoraida, B. Clara, G. Marcos, M. Rosa, S. Ricardo, *ChemSusChem*, 7(2014)914.
24. F.M. Zhao, G. Wen, L.Y. Kong, Y.Q. Chu, C.A. Ma, *Acta Phys. -Chim. Sin.*, 33 (2017) 1181.
25. F.M. Zhao, G. Wen, L.Y. Kong, Y.Q. Chu, C.A. Ma, *Chinese J. Inorg. Chem.*, 33 (2017) 501.
26. S. Ruediger, P. Alexander, M. Christian, *J. Electrochem. Soc.*, 163(2016)A2089.
27. L. Wei, T. S. Zhao, Q. Xu, X. L. Zhou, Z. H. Zhang, *Appl. Energy*, 190(2017)1112.
28. A. H. Whitehead, M. Harrer, *J. Power Sources*, 230(2013) 271.
29. Y. K. Zeng, T. S. Zhao, L. An, X. L. Zhou, L. Wei, *J. Power Sources*, 300(2015) 438.
30. B. Li, M. Gu, Z. Nie, Y. Shao, Q. Luo, X. Wei, X. Li, J. Xiao, C. Wang, V. Sprenkle, W. Wang, *Nano Lett.*, 13(2013)1330.
31. B. J. Liu, S. Q. Liu, Z. He, K. M. Zhao, J. C. Li, X. L. Wei, R. J. Huang, Y. L. Yang, *Ionics*, 25(2019)4231.
32. Z. González, A. Sánchez, C. Blanco, M. Granda, R. Menéndez, R. Santamaría, *Electrochem. Commun.*, 13(2011)1379.
33. Y. Liu, F. Liang, Y. Zhao, L. Zhao, L. Yu, L. Liu, J. Xi, *J. Energy Chem.*, 27(2018) 1333.
34. H. R. Jiang, Y. K. Zeng, M. C. Wu, W. Shyy, T. S. Zhao, *Appl. Energy*, 240(2019) 226.

35. Y. Zhou, L. Liu, Y. Shen, L. Wu, L. Yu, F. Liang, J. Xi, *Chem. Commun.*, 53(2017) 7565.
36. Y. Zhang, L. Liu, J. Xi, Z. Wu, X. Qiu, *Appl. Energy*, 204(2017)373.
37. Q. Luo, L. Li, W. Wang, Z. Nie, X. Wei, B. Li, B. Chen, Z. Yang, V. Sprenkle, *ChemSusChem*, 6(2013)268.
38. I. Derr, A. Fetyan, K. Schutjajew, C. Roth, *Electrochim. Acta*, 224(2017)9.
39. X. L. Zhou, T. S. Zhao, L. An, Y. K. Zeng, L. Wei, *J. Power Sources*, 339(2017) 1.

© 2020 The Authors. Published by ESG (www.electrochemsci.org). This article is an open access article distributed under the terms and conditions of the Creative Commons Attribution license (<http://creativecommons.org/licenses/by/4.0/>).